Molecular Therapy
Methods & Clinical Development
Original Article

# CRISPR screen reveals modifiers of rAAV production including known rAAV infection genes playing an unexpected role in vector production

Emily E. O'Driscoll,[1,2,4] Sakshi Arora,[1,3,4] Jonathan F. Lang,[1,3] Beverly L. Davidson,[1,3] and Ophir Shalem[1,2]

[1]Center for Cellular and Molecular Therapeutics, Children's Hospital of Philadelphia, Philadelphia, PA 19104, USA; [2]Department of Genetics, Perelman School of Medicine, University of Pennsylvania, Philadelphia, PA 19104, USA; [3]Department of Pathology and Laboratory Medicine, Perelman School of Medicine, University of Pennsylvania, Philadelphia, PA 19104, USA

**Recombinant adeno-associated virus (rAAV) vectors are an effective and well-established tool in the growing gene therapy field, with five U.S. Food and Drug Administration-approved AAV-mediated gene therapies already on the market and numerous more in clinical trials. However, manufacturing rAAV vectors is an expensive, timely, and labor-intensive process that limits the commercial use of AAV-mediated gene therapies. To address this limitation, we screened producer cells for genes that could be targeted to increase rAAV yield. Specifically, we performed a CRISPR-based genome-wide knockout (KO) screen in human embryonic kidney (HEK) 293 cells using an antibody specific to intact AAV2 capsids coupled with flow cytometry to identify genes that modulate rAAV production. We discovered that the KO of a group of heparan sulfate biosynthesis genes previously implicated in rAAV infectivity decreased rAAV production. Additionally, we identified several vesicular trafficking proteins for which KO in HEK 293 cells increased rAAV yields. Our findings provide evidence that host proteins associated with viral infection may have also been co-opted for viral assembly and that the genetic makeup of viral producer cells can be manipulated to increase particle yield.**

## INTRODUCTION

Recombinant adeno-associated viruses (rAAVs) are currently one of the most widely used gene delivery platforms for basic research, preclinical studies, and human gene therapies. There are currently five U.S. Food and Drug Administration-approved AAV-based gene therapy products (Luxturna in 2017, Zolgensma in 2019, Hemgenix in 2022, and Elevidys, and Roctavian in 2023) and numerous more in clinical trials.[1] Several aspects of rAAV vectors make them particularly advantageous for gene therapy. They can infect a broad range of cells in various tissues with defined specificities, which can be fine-tuned by the use of different serotypes.[2] They are able to sustain stable long-term transgene expression without the risk of random and potentially oncogenic genomic alterations. Last, while there are immunological barriers associated with rAAV delivery, these vectors are derived from a widely and naturally occurring virus that is not known to cause any human diseases.[3,4] Although dose-related toxicities can occur, it is generally considered safe for clinical use.[5,6]

Naturally occurring AAV was discovered serendipitously during lab studies of adenovirus, which is among the viruses that AAV can use as a host.[7,8] AAV is a single-stranded DNA virus with a genome of approximately 4.7 kb packed within an icosahedral protein capsid composed of the three different subunits, VP1, VP2, and VP3. The AAV genome encodes several Rep proteins required for replication, Cap capsid proteins, an assembly activating protein flanked by inverted terminal repeats that promote viral replication and packaging, and a membrane-associated accessory protein that assists in the release of viral particles from the infected cell.

In the plasmid transfection platform used to produce rAAV in human embryonic kidney (HEK) 293 cells, all protein-coding genes are removed and replaced by the delivery payload, usually gene expression cassettes with potential therapeutic value. While the HEK 293 genome already contains the essential adenovirus helper gene *E1a/b*, the majority of proteins required for viral replication and assembly must be expressed from separate plasmids. The resulting viral particles are replication incompetent, with most of their coding capacity being used for transgene delivery. These rAAV particles can then be used to transduce other cells. Their main means of entry is through binding to the AAV receptor (AAVR). AAVR, while not the only host factor involved, is crucial for rAAV entry into cells.[9,10]

One of several challenges for future widespread use and equitable access to AAV-based gene therapies is the cost and labor associated with rAAV production. Of the five currently approved therapies in the United States, one (Luxturna) targets ocular tissue and another (Zolgenzma) is for neonatal administration, which have helped to circumvent roadblocks associated with very high manufacturing

Received 31 January 2024; accepted 14 January 2025;
https://doi.org/10.1016/j.omtm.2025.101408.

[4]These authors contributed equally

**Correspondence:** Center for Cellular and Molecular Therapeutics, Children's Hospital of Philadelphia, Philadelphia, PA 19104, USA.
**E-mail:** davidsonbl@chop.edu
**Correspondence:** Center for Cellular and Molecular Therapeutics, Children's Hospital of Philadelphia, Philadelphia, PA 19104, USA.
**E-mail:** shalemo@chop.edu

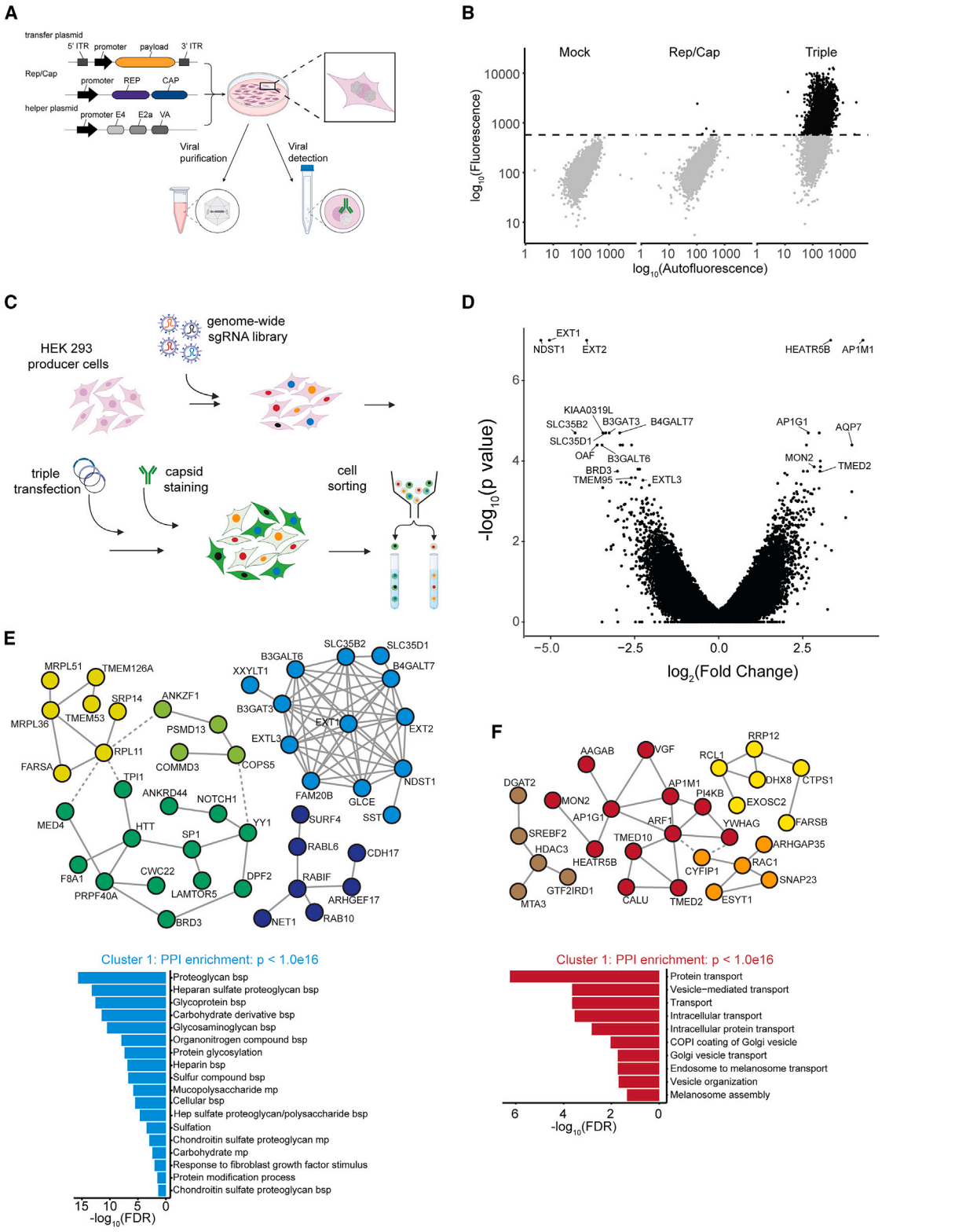


*(legend on next page)*

costs. However, many of the targets that are currently being developed are aimed at adult patients using systemic administration, which will require optimization of larger scale rAAV production practices.

It is now increasingly appreciated that rAAV particles have extensive and specific interactions with a multitude of factors in host cells. For example, the efficiency of rAAV infection depends on the interactions between the capsid proteins and cell surface receptors. Particle internalization is also mediated by several host factors involved in clathrin-mediated endocytosis, cytoskeleton-mediated endosomal trafficking, endosomal escape, and multiple routes for particle degradation.[11] Interestingly, the same factor can contribute to multiple steps in the rAAV infection life cycle. For example, AAVR, the essential receptor for multiple serotypes,[9,10] also facilitates intracellular trafficking.[12] As rAAV production is most often done in mammalian cells, it is likely that other host factors can enable or inhibit this process and can be fine-tuned to increase viral yield. Indeed, previous studies identified genes that, when overexpressed, increase production.[13,14]

Here we set out to screen for additional host factors in HEK 293 producer cells that affect rAAV production. We used CRISPR knockout (KO) screening with intracellular antibody staining specific to assembled rAAV capsids to reveal cellular pathways that negatively and positively regulate production. Surprisingly, some of the top hits for which KO decreased rAAV production were genes associated with heparan sulfate proteoglycan synthesis that were previously identified in a screen for AAV infection. We validated these results by constructing a cell line resistant to AAV infection and using it to conduct a secondary screen that identified the same top gene hits. These results suggest that AAV co-opted overlapping mechanisms for infection and intracellular viral assembly. Our screen also revealed gene knockouts that increased viral yield, suggesting that these genes encode proteins that are involved in actively opposing viral production. These included TMED2 and TMED10, which were recently identified as organizers of large protein supercomplexes at the endoplasmic reticulum (ER)-Golgi membrane. These protein supercomplexes are responsible for the transfer of cholesterol between organelles and the remodeling of plasma membrane lipid nanodomains,[15] suggesting that this process might repress intracellular AAV assembly. Finally, *MON2* KO also increased rAAV production and was previously implicated in HIV-1 viral production.[16] Altogether, we identify pathways relevant to AAV biology and show that the genome of host HEK 293 cells can be manipulated to modulate rAAV production.

## RESULTS

### Genome-wide fluorescence-activated cell sorting-based CRISPR screen reveals genetic modifiers of rAAV production

To enable genome-wide, fluorescence-activated cell sorting (FACS)-based CRISPR screening for genes that impact rAAV production, we first established a workflow for quantifying rAAV production using a cellular fluorescence-based readout that identified assembled capsids only. Typically, rAAV titers are measured after cell lysis and rAAV particle purification, but this approach is not compatible with pooled CRISPR screening. Instead, HEK 293 cells were fixed after rAAV triple transfection and stained for flow cytometry using an antibody specific to intracellular, intact assembled AAV2 capsids (Figure 1A). To ensure that the antibody was specific to assembled AAV2 particles, mock, Rep/Cap only, and triple transfected cells were fixed, stained, and flow sorted. The Rep/Cap only condition was virtually indistinguishable from the mock control condition whereas the triple transfected condition had an appreciable percentage of fluorescent cells after the optimization of staining conditions (Figures 1B and S1).

We next performed a genome-wide CRISPR-Cas9 KO screen to identify genes in producer cells that modulate rAAV production (Figure 1C). HEK 293 cells were transduced with lentiviral particles expressing SpCas9 and selected for 5 days before being transduced with a genome-wide CRISPR KO lentiviral library[17] at a low multiplicity of infection (MOI) and selected for 3 days. The cells were expanded, remaining on alternating selection for a total of 10 days to ensure expression of both the Cas9 and single guide RNA (sgRNA) and to allow time for editing. Cells then underwent rAAV triple transfection and were fixed and stained 72 h later. Stained cells were subsequently sorted based on fluorescence, collecting the 15% least and most fluorescent bins. To maintain greater than 1,000-fold coverage, cells were sorted over multiple days. After genomic DNA extraction, amplicon sequencing of the sgRNA cassette was

**Figure 1. Intracellular staining for assembled AAV2 capsids enables FACS-based measurement of rAAV production**

(A) Schematic representation of the workflow. HEK 293 cells are transfected with a transfer plasmid, AAV2 Rep/Cap, and Ad-Helper. Following triple transfection, the cells are either lysed or fixed. Cell lysis allows for the purification and quantification of AAV2 particles. Fixation followed by staining for intact AAV2 particles allows for detection of AAV2 levels by flow cytometry. (Created in BioRender. ODriscoll, E. (2025) https://BioRender.com/f36g430). (B) Mock transfected, Rep/Cap-only transfected, and triple transfected cells were fixed and stained using a primary antibody specific to intact AAV2 capsids. Flow cytometry data validated that the antibody specifically recognized assembled capsids but not unassembled Rep/Cap. (C) Screening paradigm for the genome-wide FACS-based CRISPR KO screen to identify genetic regulators of rAAV productions. HEK 293 cells were transduced first with Cas9 and then with a genome-wide sgRNA library. Following selection and expansion, the cells were triple transfected. At 72 h post-transfection, the cells were fixed and stained for assembled AAV2. The cells were then sorted, and the least fluorescent and most fluorescent cells were collected for sequencing and subsequent analysis. (Created in BioRender. ODriscoll, E. (2025) https://BioRender.com/f36g430). (D) Volcano plot displaying the phenotype on the x axis and statistical significance on the y axis with the top depleted and enriched genes annotated. (E) STRING analysis showing the protein-protein interaction clustering of the top 100 depleted genes (MCL inflation parameter = 1.5; only clusters with PPI enrichment $p < 0.001$ shown). Cluster 1, indicated in light blue, had significantly more interactions than expected by chance. Significantly enriched Gene Ontology Biological Process terms for cluster 1 are provided and show a strong enrichment in genes implicated in a proteoglycan biosynthetic process (bsp). (F) STRING analysis showing the protein-protein interaction clustering of the top 100 enriched genes (MCL inflation parameter = 1.5; only clusters with PPI enrichment $p < 0.001$ shown). Cluster 1, indicated in red, had significantly more interactions than expected by chance. Significantly enriched GO cellular component terms for cluster 1 are provided and show an enrichment in genes involved in protein transport.

performed to measure abundance of sgRNA sequences in the two collected populations.[18]

Amplicon sgRNA read counts were analyzed to generate gene-based quantifications. The phenotypic effect was measured by calculating the fold change of the average of the two top-performing sgRNAs per gene and significance was determined by calculating a *p* value using all sgRNAs per gene. The analysis revealed many genes with significant scores associated with both reduced and increased rAAV production (Figure 1D). To further investigate the pathways enriched in our primary screening results, we analyzed the top 100 gene hits in both directions using the STRING database to look for protein-protein interactions.[19] The top cluster of genes that decreased rAAV production upon KO was enriched in annotations related to proteoglycan biosynthesis, including several more specific terms related to heparan sulfate biosynthesis (Figure 1E). Interestingly, the majority of the highest-ranking genes for which KO reduced rAAV production are in this cluster and are associated with heparan sulfate biosynthesis. This includes *EXT1*, *EXT2*, *NDST1*, *B3GAT3*, and others (Figures 1D and 1E). The top 100 gene hits that increased rAAV production upon KO were enriched in cellular component annotations related to protein transport and vesicular trafficking (Figure 1F).

### Genes involved in AAV cellular entry are also implicated in rAAV production

Of the genes for which KO decreased rAAV production, both the STRING and g:Profiler analyses highlighted a group of heparan sulfate biosynthesis-related genes (Figures 1E and S2).[19,20] Membrane-associated heparan sulfate proteoglycans play an established role in AAV2's ability to bind to and infect cells,[21,22] and this same group of genes was identified in a previously published screen for genetic regulators of AAV2 cellular entry.[9]

With this in mind, we colored the depletion arm of our AAV2 production screen based on the groups of genes implicated in this previous screen for AAV2 cellular entry.[9] Of the eight previously implicated heparan sulfate biosynthesis genes, seven of them were among our highest-ranked gene hits. In fact, these heparan sulfate genes and the *AAVR* gene made up the majority of our top hits (Figure 2A). We, therefore, wondered if some of the rAAV2 produced was being secreted into the media and infecting our cells before sorting. This seemed unlikely since other genes implicated in mediating AAV2 infectivity did not seem to modulate rAAV production in our screen (Figures 2A and S3). Still, to further exclude this possibility, we generated a clonal AAVR KO line (Figure 2B). While *AAVR* is not the only gene involved in AAV2's cellular internalization, it is required for efficient AAV2 infectivity.[9,10,12] As such, transduction of our clonal AAVR KO line with rAAV containing a GFP transfer plasmid showed little green fluorescence as compared with wildtype cells (Figure 2C). This suggests that the clonal AAVR KO line cannot be readily transduced by rAAV.

Next, we used the clonal AAVR KO line to perform a focused secondary CRISPR KO screen (Figure 2D). The use of this AAVR KO line allowed us to screen for regulators of rAAV production without the risk of rAAV infection of the producer cells confounding our results. This targeted library contained eight sgRNAs each for the top genes identified from the genome-wide screen. The clonal AAVR KO line was transduced with Cas9 followed by the targeted sgRNA library, and the screen was performed as described for the genome-wide screen. The only exception was that the cells were fixed 48 h post-AAV transfection instead of at 72 h to further reduce the possibility of reinfection.

In the depletion arm of this focused screen in AAVR KO cells, AAVR was no longer a hit, as expected. However, heparan sulfate biosynthesis genes remained as top hits, suggesting that their role in rAAV production is independent of their role in AAV2 cellular entry (Figure 2D). We next took three of the highest-ranked heparan sulfate biosynthesis genes and tested them in an arrayed format (Figure 2E). Two sgRNAs each for *B3GAT3*, *B4GALT7*, *EXT1*, and the control locus *CLYBL* were used to KO their respective gene in wildtype HEK 293 cells in duplicate. The lines then underwent rAAV triple transfection and were subsequently fixed, processed, and flow sorted to quantity assembled AAV2 capsid levels. Compared with the *CLYBL* control, all three heparan sulfate biosynthesis genes tested showed a significant decrease in median fluorescence intensity, suggesting a decrease in AAV production upon KO. Specifically, AAV production decreased by an average of 23% for B3GAT3 KO, 33% for B4GALT7 KO, and 26% for EXT1 KO. We next tested the transfection efficiency and cell viability of additional B3GAT3, B4GALT7, and EXT1 KO lines and found that they were indistinguishable from the CLYBL control lines (Figure S4), supporting that KO of these genes directly impact AAV production.

To further validate the role of heparan sulfate biosynthesis genes in rAAV production using an orthogonal gene perturbation approach, we electroporated wildtype HEK 293 cells with RNPs containing Cas9 protein and an sgRNA against EXT1 (Figures 2F–2H). As a control, we electroporated HEK 293 cells with Cas9 protein only. Our polyclonal EXT1 KO populations showed a high level of editing efficiency (Figure 2F). AAV-transfected EXT1 KO cells had a significant decrease in median fluorescent levels compared with controls, indicating EXT1 KO decreased rAAV production by an average of 56% (Figure 2G). We further quantified the effect of EXT1 KO by using qPCR for the payload and normalizing it to Gaussia luciferase as a control for transfection efficiency (Materials and methods). We found that EXT1 KO producer cells had approximately 23% less rAAV yield when quantified using qPCR (Figure 2H). While this decrease in yield was less than seen with FACS, this is likely due to methodological differences between the two assays. The FACS assay stains for all assembled capsids, meaning it is a readout of both empty and full AAV2 capsids. The qPCR assay measures the payload, implying that it is a readout of only non-empty AAV2 capsids.

To test the functionality of rAAV produced in EXT1 KO producer cells, the viral particles produced in the EXT1 KO lines were then used to transduce wildtype HEK 293 cells. Transduction efficiencies were indistinguishable from AAV produced in wildtype cells

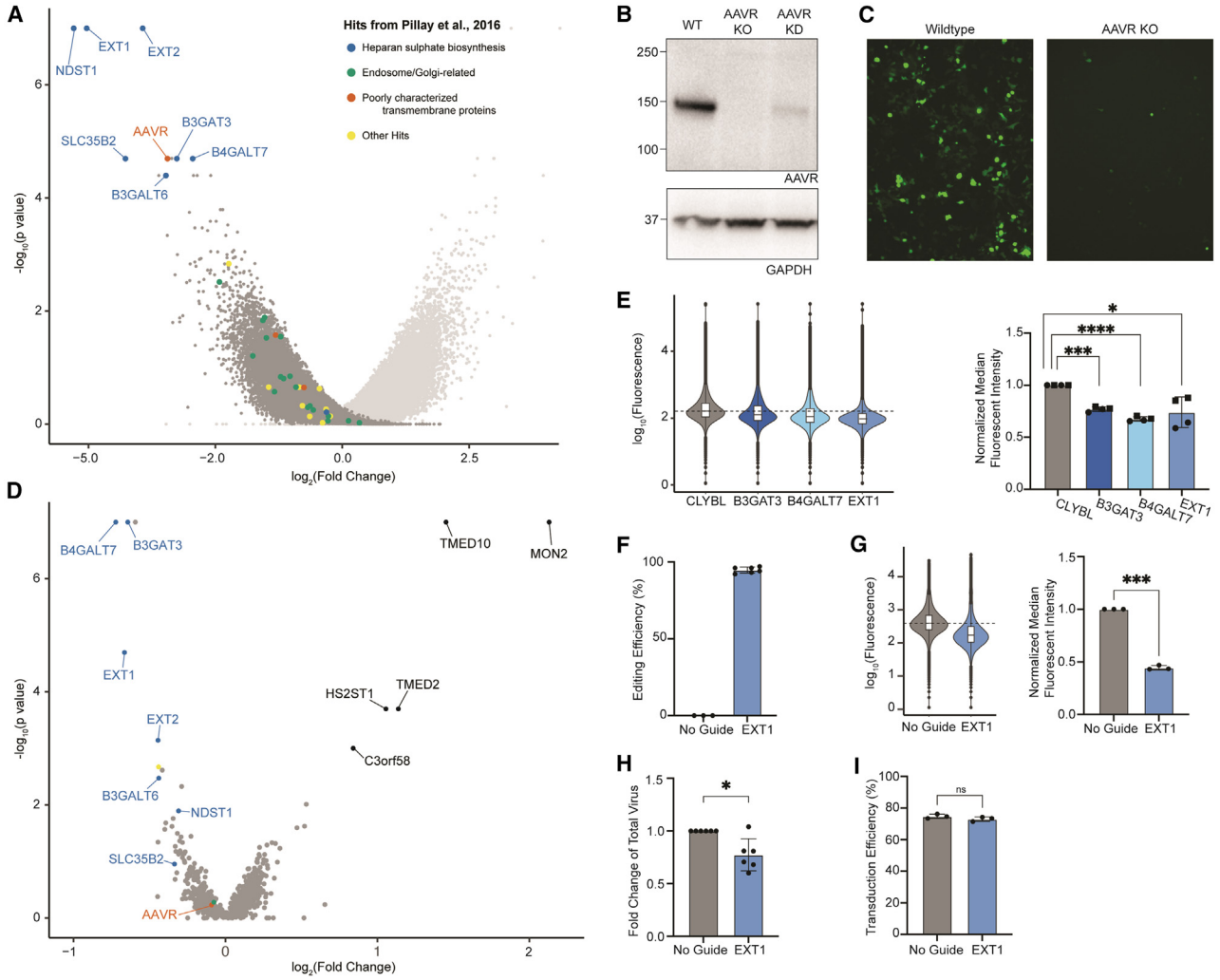


**Figure 2. Genes implicated in AAV infection are involved in rAAV production**

(A) The depletion arm of the rAAV production screen's volcano plot is colored based on genes implicated in AAV infection from Pillay et al. (2016). (B) AAVR KO clonal HEK 293 line confirmed by western blot. (C) AAV-GFP transduction in wildtype HEK 293 and AAVR KO clonal lines. (D) Secondary screen of the top hits from the genome-wide rAAV production screen. The volcano plot is colored by the previously published AAV infectivity screen. (E) FACS-based quantification of rAAV production in polyclonal KO lines generated using lentiviral-delivered Cas9 and sgRNA. Two sgRNAs were tested per gene (denoted with circle and square points) in duplicate for a total of four replicates per gene. A representative FACS plot from one replicate is shown in addition to the normalized median fluorescent intensities. B3GAT3 ($p = 0.0003$), B4GALT7 ($p < 0.0001$), and EXT1 ($p = 0.0383$) all significantly decreased rAAV levels compared with CLYBL. (F) Polyclonal EXT1 KO lines were generated by electroporation of Cas9/sgRNA RNPs and compared with HEK 293 cells electroporated with only Cas9. Editing efficiency was quantified by Sanger sequencing followed by ICE analysis. (G) rAAV production was measured by FACS for three EXT1 KO lines and three control lines. A t test was performed, and there was a significant ($p = 0.0005$) decrease in median fluorescent intensity upon EXT1 KO compared with control. (H) rAAV production was measured by qPCR for six EXT1 KO lines and six control lines. A t test was performed, and EXT1 KO led to a significant ($p = 0.0152$) decrease in viral levels. (I) AAV particles containing GFP as the transgene were produced in three EXT1 polyclonal KO lines. This AAV-GFP was used to transduce wildtype HEK 293 cells, and transduction efficiency was assessed by flow cytometric-based quantification. Based on a t test, there was no significant difference in transduction efficiency for rAAV produced in EXT1 KO lines compared with control ($p = 0.2129$). All error bars in this figure represent the standard deviation from the mean.

electroporated with Cas9 only (Figure 2I). This suggests that, while KO of EXT1 in producer cells reduces viral yield, it does not alter the functionality of the rAAV particles.

### Related vesicular trafficking proteins modulate rAAV production

The focused secondary screen in the clonal AAVR KO line also brought several genes to our attention for which KO increased rAAV yields (Figure 2D). The top 10 genes consisted of known protein-protein interactors and were enriched in annotations related to vesicular protein trafficking (Figure 3A). We took the top three genes and tested them in an arrayed format. We first generated polyclonal KO lines of TMED2, TMED10, and MON2 using lentiviral-delivered Cas9 and sgRNAs. These polyclonal lines showed no difference in transfection efficiency or cell viability compared with CLYBL control

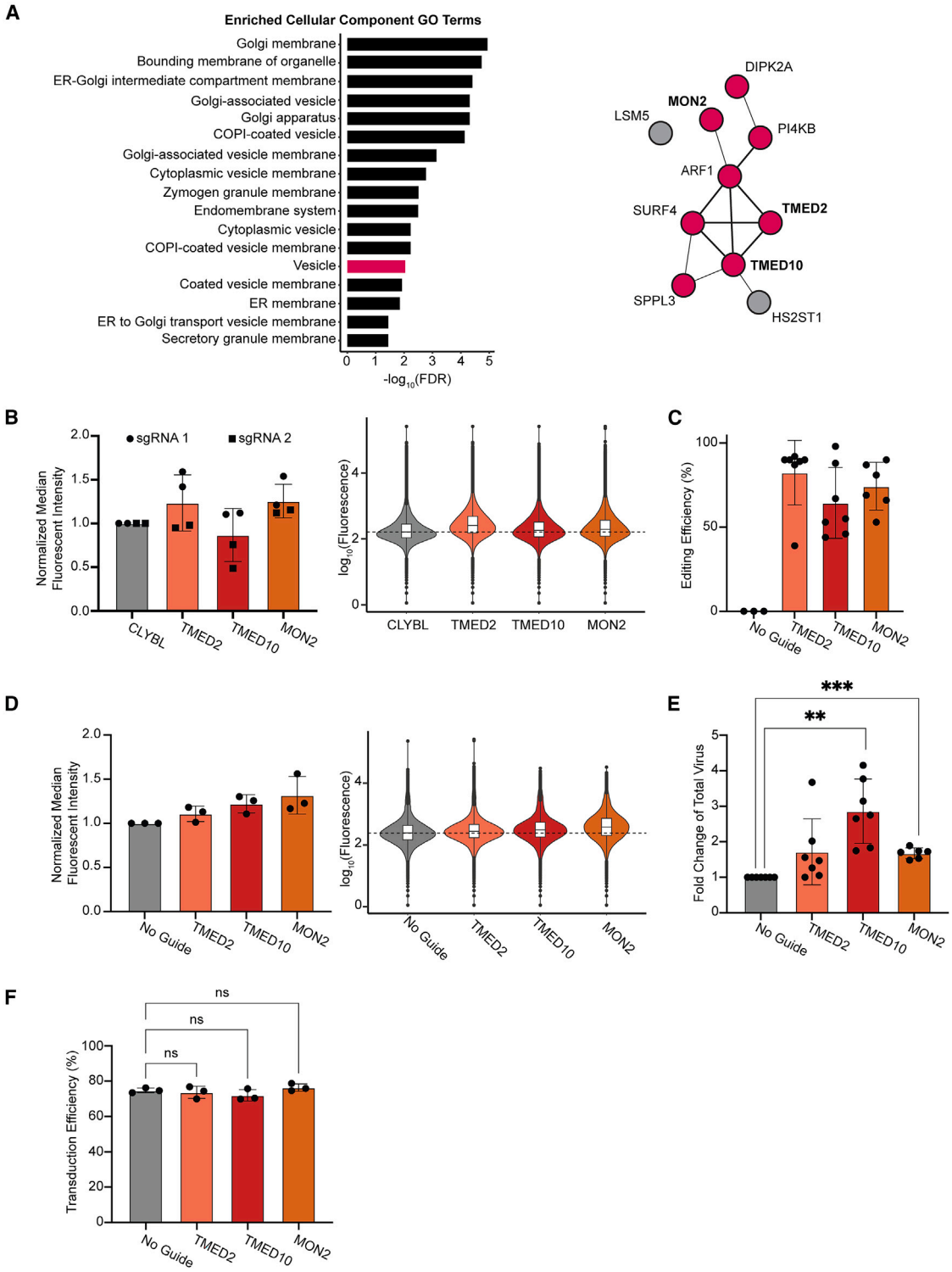


**Figure 3. Network analysis identifies trafficking proteins that modulate AAV production**

(A) STRING analysis showing all potential protein-protein interactions (with interaction scores of >0.150) between the top 10 hits from the secondary screen where gene KO increased rAAV production. Significantly enriched Gene Ontology (GO) terms included many vesicle-related annotations. (B) FACS-based quantification of rAAV production in polyclonal KO lines generated using lentiviral-delivered Cas9 and sgRNA. Two sgRNAs were tested per gene (denoted with circle and square points) in duplicate for a total of

*(legend continued on next page)*

(Figure S4), suggesting that their effect on rAAV production was direct. We next quantified rAAV production using our FACS-based approach (Figure 3B). While some sgRNAs showed a trend toward increased rAAV production, there was large sgRNA-dependent variability likely associated with differences in gene editing efficiency and variability in small-scale rAAV production.

Therefore, to achieve higher KO efficiency, we tested all three genes using the orthogonal RNP-based approach described in the previous section. The editing efficiency of the TMED2, TMED10, and MON2 lines varied but averaged 82%, 64%, and 74%, respectively (Figure 3C). Any lines with editing below 10% were excluded from further analysis. rAAV production in these lines was quantified using both the FACS-based and qPCR-based methods and was compared with wildtype cells electroporated with only Cas9. KO of either TMED2, TMED10, or MON2 trended toward an increase in fluorescence as measured by FACS (Figure 3D). When quantified by qPCR, TMED10 KO produced 2.86 times more AAV2 than control and MON2 KO increased AAV2 production 1.68-fold (Figure 3E). Furthermore, virus produced in the KO lines was used to transduce wildtype HEK 293 cells, and there was no significant difference in the transduction efficiency compared with when control virus was used (Figure 3F), suggesting that the virus produced in these KO lines is functional. Thus, KO of TMED2, TMED10, or MON2 in producer cells may be a useful tool for increasing the production of functional AAV2. While this screen focused on regulators of AAV2 production, it is possible that these hits could be more broadly applicable to other serotypes. Preliminary tests of AAV8 and AAV9 production in our RNP-generated KO lines suggest that TMED2 and TMED10 KO may also increase AAV8 and AAV9 production (Figure S5).

## DISCUSSION

Current costs and labor associated with rAAV production are one roadblock to providing wide access to rAAV-mediated gene therapies. We hypothesized that modification of the genetic makeup of producer cells can affect rAAV yield and be used to fine-tune production. To test this hypothesis, we performed a FACS-based genome-wide CRISPR KO screen for rAAV production using an antibody that only recognizes assembled AAV2 capsids. Our choice to use AAV2 was driven by the fact that, unlike other serotypes, the AAV2 serotype is not readily secreted into the media when produced in HEK 293 cells. Additionally, an antibody existed that allowed us to specifically recognize assembled AAV2 capsids by flow cytometry instead of being limited to looking at total capsid protein levels. This facilitated a pooled screening approach in which the level of assembled AAV2 particles in single cells could be mapped to sgRNA perturbations.

Interestingly, a vast majority of the genes for which KO reduced rAAV production were associated with heparan sulfate biosynthesis and were all previously identified in a screen for AAV infection (Figure 2A).[9] Other genes that were identified in the AAV infection screen (Figure 2A) or in other studies (Figure S3) that were not associated with heparan sulfate biosynthesis did not seem to be associated with rAAV production, suggesting that these findings are not due to the technical limitations of our experimental system. Still, to further validate the results, we generated clonal HEK 293 producer cells that lack AAVR and are thus resistant to AAV infection. Reassuringly, conducting a secondary screen in those lines reproduced these results, raising the interesting hypothesis that heparan sulfate biosynthesis, a process that is essential for AAV infection, has also been co-opted by AAV for efficient intracellular assembly. More work is required to understand the mechanisms that underlie this dependency and if overactivation of this pathway can be used for increased rAAV production.

Our screen also identified genes whose loss resulted in increased rAAV production. Indeed, several genes associated with vesicular trafficking came up as strong hits in both our primary and secondary screens. Of specific interest were TMED2 and TMED10, two proteins with a well-established interaction that are components of a protein complex localized at the ER-Golgi interface and among the p24 family of proteins involved in the biogenesis of COPI and COPII-coated vesicles.[23] Interestingly, TMED2/10 were identified in a screen for anthrax intoxication,[15] further connecting cellular internalization pathways with intracellular assembly. Loss of TMED2/10 affected cholesterol transport between organelles and resulted in aberrant Golgi morphology. Therefore, TMED2/10 KO may impact the ability of producer cells to degrade full or partially assembled capsids. Future work will assess if stronger inhibition of this pathway by knockdown of more than one gene can further improve rAAV production compared with KO of TMED2 or TMED10 alone.

While our CRISPR-Cas9 KO screening method proved to be a powerful tool for identifying regulators of intact assembled rAAV2 capsid production, it does come with certain limitations. Most notably, the antibody used in the screen detects empty AAV2 capsids equally as well as AAV2 particles containing the viral genome, meaning that we are unable to distinguish between full and empty capsids. Not all assembled capsids will contain the vector genome, and these empty capsids are not of therapeutic use. Therefore, genes that could be

four replicates per gene. A representative FACS plot from sgRNA 1 is shown in addition to the normalized median fluorescent intensities. (C) Polyclonal KO lines were generated by electroporation of Cas9/sgRNA RNPs and compared with HEK 293 cells electroporated with only Cas9. Editing efficiency was quantified by Sanger sequencing followed by ICE analysis. (D) rAAV production was measured by FACS for three KO lines each for TMED2, TMED10, and MON2 and compared with three control lines. (E) rAAV production was measured by qPCR for six KO lines per gene and compared with six control lines. Both TMED10 ($p = 0.0016$) and MON2 ($p = 0.0001$) significantly increased rAAV production. (F) Flow cytometric-based quantification of wildtype HEK 293 cells transduced with AAV-GFP produced in polyclonal KO lines. There was no significant difference in transduction efficiency for rAAV produced in TMED2 ($p = 0.9330$), TMED10 ($p = 0.4918$), or MON2 ($p = 0.7960$) KO lines compared with control. All error bars in this figure represent the standard deviation from the mean.

manipulated in the producer cells to increase the percentage of rAAV particles that contain the vector genome would be of interest, even if the total rAAV yield remained the same. These genes would not have been identified in our screen. Additionally, while we validated that our top hits modulate total rAAV production, further studies are needed to quantify to what extent this is driven by a change in the number of full particles.

Another challenge we faced was the inherent variability in rAAV production. Arrayed testing of rAAV production depends on many experimental factors including but not limited to cell density, growth phase, and transfection efficiency, which contributed to the high variability seen in the small-scale arrayed experiments we used to validate our top hits. In a sense, pooled screens with sufficient cell and sequencing coverage can provide more accurate ranking of gene knockouts, as cells with different perturbations grow within the same plate experiencing precisely the same culturing and treatment conditions. Because of the variability in our assay readout, validation was best achieved using RNP knockouts of TMED2, TMED10, and MON2 compared with polyclonal lentiviral-based validation studies. This approach yielded higher KO efficiency and avoided the effect of selection on cell growth and viability.

Last, as our work aimed to increase rAAV yield at production scale, we envision two ways in which such data can be incorporated into standard production pipelines. The first is by engineering producer cell lines with genetically modified genomes and the second is by transient knockdowns during viral production. For the former method, since clonal selection alone can introduce large variation in cell growth and rAAV production capabilities, any derived clones with specific gene knockouts would need to be compared with a population of clones previously optimized for production without any targeted mutations. Additionally, large-scale rAAV manufacturing is increasingly using suspension-adapted HEK 293 cells, and future studies into whether our top hits will validate in these non-adherent lines would add to their applicability. In summary, our work presents pathways that can be co-opted to improve rAAV production, with practical applications to the adoption of AAV gene therapies more broadly.

## MATERIALS AND METHODS

### Molecular cloning

#### *Individual sgRNAs for lentiviral-mediated CRISPR KO*

The two sgRNA sequences with the highest fold-changes in the screens were used for targeted screen validation. The forward and reverse sgRNA sequences were ordered as primers. The sgRNA oligos were phosphorylated and annealed before being inserted by Golden Gate cloning into BsmBI cloning sites in lentiGuide-Puro (Addgene 52963).

### Cell culture

#### *Maintenance*

HEK 293 cells (ATCC CRL-1573) were maintained in DMEM (Gibco 11995065) with 10% FBS and 1% NEAA (Gibco 11140076). Cells were grown at 37°C with 5% $CO_2$ to maintain physiological pH. Cells were tested regularly for mycoplasma contamination.

#### *Lentiviral generation*

Human 293Ts (ATCC CRL-3216) were plated such that they would be 75% confluent at the time of transfection in plates coated with 0.1% gelatin. Between 30 and 60 min before transfection, the media was changed using DMEM with 10% FBS, 1% NEAA, and 1% HEPES, and 70% of the standard volume was used. Lentivirus for individual sgRNAs was prepared in six-well plates by co-transfecting 293Ts with 1.06 μg pMDLG (Addgene #12251), 0.57 μg pMD2G (Addgene #12259), 0.4 μg pRSV-Rev (Addgene #12253), 1.06 μg plasmid to be packaged, 100 μL Opti-MEM, and 7.35 μL PEI per individual well. Lentivirus for pooled libraries was prepared in 15-cm plates by co-transfecting 293Ts with 13.25 μg pMDLG, 7.2 μg pMD2G, 5 μg pRSV-Rev, 20 μg of pooled library (Brunello Library Addgene #73178 or lab-cloned secondary library), 3 mL Opti-MEM, and 136 μL PEI per plate. At 5 to 6 h after transfection, the media was changed to DMEM with 10% FBS and 1% NEAA. At 48 h after transfection, the supernatant was collected and filtered through a 0.45-μM filter. The supernatant was aliquoted and stored at −80°C until use. Lentivirus was thawed on ice before transduction.

#### *AAV triple transfection*

Human 293 cells (ATCC CRL-1573) were seeded at 40,000 cells per 12-well well 1 day before transfection such that they would be 80%–90% confluent at the time of transfection. The next day, rAAV particles were produced using standard three plasmid co-transfection (Wright[24]). We used standard pAd Helper (Addgene), AAV2 rep/cap (Addgene), and an AAV shuttle plasmid expressing the indicated transgenes under the CAG promoter. For the SpCas9 transgene, we used the PX551 plasmid from Addgene. The pTransgene used were as follows: luciferase for both screens, mRuby3 and SpCas9 for all FACS-based arrayed assays, and eGFP and SpCas9 for all qPCR-based arrayed assays. The three plasmids were transfected in a 1:1:1 M ratio (total DNA = 1.5 μg per well) using PEI Max. Briefly, the required amount of DNA was added to 10 μL (per well) of Opti-MEM. In another tube 3.0 μL of PEI Max was added to 10 μL (per well) of Opti-MEM and mixed well. PEI Max/Opti-MEM was added to DNA/Opti-MEM, pipetted up and down several times, and incubated for 15 min at room temperature (RT). We added 20 μL of transfection mix to each well and the cells were incubated at 37°C. At 24 h later, the media of the cells was replaced with DMEM-5 (DMEM with 10% FBS and 1% penicillin-streptomycin). For the RNP experiments analyzed by qPCR (Figures 2H and 3E), we included secretary Gaussia luciferase as an additional control. For this, 0.1 μg of pMCSGaussia-Dura Luc Vector (Thermo Fischer Scientific) was transfected per well and 100 μL of the supernatant was collected 24 h after transfection to perform the luciferase assay. Note that, for all arrayed experiments of the top hits (Figures 2E–2I and 3B–3E), each data point represents a unique polyclonal line that was triple/quadruple transfected to produce AAV.

#### *Fixing and staining AAV-transfected cells for flow cytometry*

AAV-transfected cells were lifted 48 or 72 h after AAV triple transfection and fixed and permeabilized using the BD Cytofix/Cytoperm Fixation/Permeabilization Kit (554714). For the screens, 1 mL of solution/buffer was used per 10 million cells. For validation experiments, 500 μL of solution was used per well. After fixation and permeabilization according to the kit instructions, cells were incubated with primary antibody against assembled AAV2 capsids (1:50; American Research Products 03–61055), washed using BD Perm/Wash Buffer, incubated with secondary antibody (1:200; Invitrogen A-11001), washed using BD Perm/Wash Buffer, and resuspended in PBS. Cells were stored at 4°C overnight before being subjected to flow cytometry.

#### *Gaussia luciferase assay*

Gaussia luciferase activity was measured in the supernatant according to the manufacturer's instructions (Pierce Gaussia Luciferase Glow Assay Kit, Thermo Fisher Scientific). Briefly, 20 μL of 1:20 diluted supernatant was added to a 96-well plate followed by 50 μL of the working solution. The plate was incubated at RT for 10 min and luminescence intensity was measured using a luminometer at a signal integration of 500 ms.

#### *Quantifying AAV production*

At 72 h after transfection, cells were harvested in PBS-MK (1 mM $MgCl_2$ and 2.5 mM KCl) buffer (1 mL per 12-well well). Cell lysis was performed using four freeze-thaw cycles. Lysates were then treated with 50 U/mL of Benzonase for 1 h at RT. Lysates were then centrifuged at 15,000×*g* for 10 min to remove protein and cellular debris. We then treated 2 μL of each sample with DNAse for 2 h at 37°C followed by heat inactivation. AAV particles were lysed using 50 μL of lysis buffer and incubated at 95°C for 10 min. Samples were then diluted 1:500 and vector yields was calculated using qPCR using a standard curve. Primer/probes were designed specific to the transgene.

### Cell line engineering

#### *Polyclonal Cas9-expressing 293 cells*

For the CRISPR KO screens and all lentivirus-mediated gene KO experiments, low-passage 293 cells were transduced with lentiCas9-Blast (Addgene# 52962). In individual wells of six-well plates, 0.5 million 293 cells were transduced with 100 μL of lentiCas9-Blast lentivirus in media containing polybrene (Sigma TR1003G, 1:1,000). At 24 h post-transduction, the transduced cells were selected using Blasticidin (5 μg/mL; Thermo Fisher Scientific A1113903) for 5 days.

#### *Clonal AAVR KO line*

Polyclonal Cas9-expressing 293 cells were transduced with an sgRNA targeting the AAVR as described in the section above. Following puromycin selection, the cells were single-cell sorted and clones were expanded. Clonal lines were first screened using Sanger sequencing and ICE analysis to identify clones with editing at the AAVR locus.[25] Promising clones were further screened by western blot to identify a clone with no AAVR expression.

#### *Western blot*

Cells were lysed in RIPA buffer (50 mM Tris-HCl, pH 8, 150 mM NaCl, 1% IGEPAL CA-630, 0.5% sodium deoxycholate, 0.1% SDS) supplemented with 1× cOmplete Protease Inhibitors (Roche). Samples were incubated on ice for 30 min then spun at >18,000×*g* for 20 min at 4°C. Supernatant protein concentration was measured using a BCA kit. Fifty micrograms were loaded into 4%–12% Criterion XT Bis-Tris gels (Bio-Rad) and transferred to PVDF membranes for blotting. Membranes were blocked for 1 h at RT in 5% BSA in 1× TBST (137 mM NaCl, 2.7 mM KCl, 19 mM Tris Base, 0.1% Tween 20). The blot was cut into two halves at 76 kDa. The top one-half was incubated with mouse anti-AAVR (KIAA0319L) diluted 1:1,000 in 5% BSA in TBST and lower one-half in mouse anti-GAPDH diluted 1:2,000 in 5% BSA in TBST for 2 h at RT followed by three washes. The blots were then incubated with goat anti-mouse IgG HRP (Thermo Fisher Scientific) diluted 1:10,000 in 5% BSA in TBST for 1 h at RT. Following washes, membranes were exposed using ECL Prime Western Blotting Detection Reagent (Cytiva).

#### *Validation of the clonal AAVR KO line*

The clonal AAVR KO HEK 293 line was transduced with AAV-GFP virus (AAV2/1-CMV-eGFP-WPRE) at an MOI of 1e5 genome copies per cell. Wildtype HEK 293 cells were transduced as a control. The cells were imaged via fluorescence microscopy at 24 and 48 h after transduction.

#### *Clonal AAVR KO line stably expressing Cas9*

The AAVR clonal line generated above was transduced with lenti-Cas9-Blast (Addgene# 52962). In individual wells of six-well plates, 0.5 million 293 cells were transduced with 100 μL of lentiCas9-Blast lentivirus in media containing polybrene (Sigma TR1003G, 1:1,000). At 24 h post-transduction, the transduced cells were selected using Blasticidin (5 μg/mL; Thermo Fisher Scientific A1113903) for 5 days.

#### *Targeted polyclonal KO lines generated using Cas9 and sgRNA lentiviruses*

The Cas9-expressing 293 cell line was transduced with sgRNA lentivirus targeting an individual gene locus. Loci targeted included the top-ranked genes from the focused secondary screen and the CLYBL locus as a control. The two top-ranked sgRNAs from the screens were tested for each gene. Cells were transduced by adding lentivirus and polybrene (Sigma TR1003G, 1:1000) to the cells in suspension. At 24 h after transduction, the transduced cells were selected using puromycin (1 μg/mL, Thermo Fisher Scientific #A1113803) for 3 days.

#### *Targeted polyclonal KO lines generated using electroporation of RNPs*

For RNP-based KO of genes for targeted validation experiments, Cas9 and sgRNAs were ordered from IDT. Alt-R S.p. Cas9 Nuclease V3 was used (IDT 1081059), and the top-recommended sgRNA was chosen for each hit (IDT Alt-R CRISPR-Cas9 sgRNA; Hs.Cas9.EXT1.1.AA, Hs.Cas9.MON2.1.AA, Hs.Cas9.TMED10.1.AA, and Hs.Cas9.TMED2.1.AA). As a control, a condition was included

without an sgRNA. To assemble the RNPs, 104 pmol of Cas9, 120 pmol of sgRNA, and PBS were brought to a total volume of 5 μL. This was incubated at RT for 20 min and then put on ice until electroporating. Electroporation was then performed using the Neon transfection system (Thermo Fisher Scientific). We resuspended the 293 cells in Resuspension Buffer R (Neon) and then mixed them with the RNP. They were then immediately electroporated with 1 pulse at 1,500 V for 30 ms using Electrolytic Buffer E (Neon). Following recovery, cells were expanded and evaluated for genome editing and AAV production on day 10. To assess quantitative editing, genomic DNA was isolated, and the target region was PCR amplified and Sanger sequenced. The percentage of cells edited was determined using ICE analysis.[25] Polyclonal lines with editing efficiencies below 10% were discarded. AAV production was evaluated in the cells as described earlier.

### CRISPR KO screens in 293 for AAV production

#### *Genome-wide library plasmid preparation*

Brunello genome-wide sgRNA library containing an average of 4 sgRNAs per gene and 1,000 non-targeting control sgRNAs was purchased from Addgene (73178). The library was transformed into electrocompetent cells (Lucigen 60242-1) and recovered at 32°C for 16–18 h to prevent recombination. Plasmid DNA was sequenced to confirm library distribution and sgRNA representation.

#### *Focused secondary library plasmid preparation*

A library of 3,012 sgRNA sequences was synthesized by Twist and contained 500 non-targeting sgRNAs and 2,512 sgRNAs targeting the top hits from the genome-wide screen (approximately eight sgRNAs per gene for the top genes identified in each arm of the genome-wide screen). The pool of sgRNA sequences was PCR amplified and inserted into lentiGuide-Puro (Addgene 52963) via Golden Gate cloning. The library was transformed into electrocompetent cells (Lucigen 60242-1) and recovered at 32°C for 16–18 h to prevent recombination. Plasmid DNA was sequenced to confirm library distribution and sgRNA representation.

#### *Lentivirus titering in 293s*

To ensure a low MOI lentiviral transduction, library sgRNA lentivirus was titered. For the genome-wide screen, Brunello library (Addgene 73178) virus was titered in 293 stably expressing Cas9. For the focused secondary screen, the lab-cloned secondary library virus was titered in the 293 AAVR KO clonal line stably expressing Cas9. Library lentivirus was titered by plating $2 \times 10^6$ cells per well of a 12-well plate with increasing volumes of virus mixed while the cells were in suspension along with polybrene infection reagent (Sigma TR1003G, 1:1,000). Plates were spinfected by centrifugation at 1,000×*g* for 1 h at 37°C. After approximately 16 h, each well was split into duplicate wells: one without treatment and one treated with puromycin (1 μg/mL, Thermo Fisher Scientific A1113803). After 3 days, cells from each well were lifted and counted, and the ratio of live cells in the wells with or without puromycin was calculated. The virus volume that achieved approximately 30% cell survival after puromycin treatment was used for the screen.

#### *FACS-based CRISPR KO screens for AAV production*

For the genome-wide screen, low-passage 293 cells expressing Cas9 were grown to approximately 85% confluency before being lifted and counted. To achieve greater than 1,000× coverage, $288 \times 10^6$ cells were mixed with polybrene infection reagent (Sigma TR1003G, 1:1,000) and the Brunello genome-wide sgRNA library virus at low MOI (using the titer calculated above). After thoroughly mixing, $2 \times 10^6$ cells were plated per well in 12-well plates and spinfected by centrifugation at 1,000×*g* for 1 h at 37°C. After overnight incubation, all of the cells were lifted, counted, and plated in 15-cm plates at $7 \times 10^6$ cells per plate. Puromycin (1 μg/mL, Thermo Fisher Scientific A1113803) was added to select for transduced cells. Cells were split every 3–4 days over the next 14 days. They were maintained on alternating puromycin and blasticidin selection the entire time. At each split, cells were counted and $160 \times 10^6$ cells were replated across 20 × 15-cm plates. All remaining cells were discarded.

On day 14, the cells were lifted, counted, and plated to be 75% confluent 24 h post-plating. The following day, the cells underwent AAV triple-transfection using pAAV2-Rep/Cap, pAdeno-Helper, and CBA-luciferase and PEI. 72 h after AAV transfection, the cells were harvested, fixed, and stained for assembled AAV capsids. Cells were then filtered through a 35μm filter (Falcon, 352235) before FACS analysis and collection. Cells were gated to have a narrow range of FCS and SSC values to select for live, single cells. Autofluorescence was detected by the 405-nm laser and 450/50 filter. The fluorescence of the antibody for assembled AAV capsids was detected using the 488-nm laser and 515/510 filter. The top and bottom approximately 20% of fluorescent cells were collected. Sorted cells were pelleted and stored at −20°C until DNA extraction.

For the focused secondary screen, clonal AAVR KO 293 cells expressing Cas9 were transduced with the secondary library virus. To maintain greater than 1,000× coverage, $42 \times 10^6$ cells were mixed with polybrene infection reagent (Sigma TR1003G, 1:1,000) and secondary library virus at a low MOI (as calculated in the section above). After thoroughly mixing, $2 \times 10^6$ cells were plated per well in 12-well plates and spinfected by centrifugation at 1,000×*g* for 1 h at 37°C. After overnight incubation, all of the cells were lifted, counted, and plated in 15-cm plates at $7 \times 10^6$ cells per plate. Puromycin (1 μg/mL, Thermo Fisher Scientific A1113803) was added to select for transduced cells. Cells were split every 3–4 days and kept on puromycin selection for the first 4 days followed by 5 days of blast selection. At each split, cells were counted and $70 \times 10^6$ cells were replated across 7 plates. All remaining cells were discarded.

At 24 h before AAV triple transfection, 7 gelatin-coated 15-cm plates were plated with 15 million cells each. At 45 min before transfection, the media was changed with 15 mL using DMEM with 10% FBS, 1% NEAA, and 1% HEPES. Each plate was co-transfected with 750 μL containing Opti-MEM, 18.08 μg pAAV2-Rep/Cap, 27.68 μg pAdeno-helper, 14.23 μg CBA-luciferase, and 120 μL PEI. Media was changed 6 h later. At 48 h after AAV triple transfection, cells were harvested, fixed, and stained for assembled AAV capsids. Cells

were sorted as described for the genome-wide screen above. A total of $6 \times 10^6$ of the least fluorescent cells and $7.8 \times 10^6$ of the most fluorescent cells were collected. Sorted cells were pelleted and stored at −20°C until DNA extraction.

#### *DNA extraction, PCR amplification, and next-generation sequencing*

Cell pellets were thawed on ice then resuspended in 3 mL lysis buffer (50 mM Tris, 50 mM EDTA, 1% SDS, pH 8). After resuspension, 15 μL proteinase K (Qiagen 19131) was added to each sample. Samples were incubated at 55°C overnight. After overnight incubation, 15 μL of diluted RNase A (Qiagen 19101, 10 mg/mL) was added to each sample and mixed thoroughly. Samples were then incubated for 30 min at 37°C. Samples were immediately placed on ice after incubation with RNaseA, where 1 mL pre-chilled 7.5M ammonium acetate was added to cooled samples to precipitate proteins. The samples were then vortexed for 30 s at top speed and spun at 4,000×*g* for 10 min. The supernatant was then transferred to fresh tubes, where 4 mL 100% isopropanol was added to precipitate the genomic DNA. Tubes were inverted 50 times and centrifuged again at 4,000×*g* for 10 min. The supernatant was decanted and 3 mL 70% ethanol was added to further purify the genomic DNA. Samples were inverted 10 times and spun at 4,000×*g* for 1 min to pellet the DNA. As much of the supernatant was removed as possible before allowing the genomic DNA to air dry for 2 h. It was then resuspended in 200 μL of nfH2O and incubated at 65°C for 1 h followed by RT overnight to fully resuspend the DNA. DNA was then quantified by Nanodrop.

sgRNA sequences were PCR amplified with custom primers targeting the genome-integrated sgRNA backbone and containing Illumina adapters and unique barcodes for each sample to allow for multiplexing. PCR products were gel extracted and quantified by Qubit dsDNA HS assay (Thermo Fisher Scientific Q32851). All samples were then pooled in equimolar ratios and sequenced using Illumina NextSeq 500/500 v2 75 cycle kit (Illumina 20024906). Amplifications were carried out with 1x8 cycles for sample index reads and $1 \times 63$ cycles for the sgRNA.

#### *Screen data analysis*

Raw fastq files were trimmed to remove sequences that flank the 20 bp and mapped to the sgRNA library using Bowtie. sgRNA counts were then loaded to R and the following steps were performed to calculate a phenotype and *p* value for each gene. Counts were first normalized by read depth by dividing read count by sample mean, multiplying by a million and adding 1 pseudocount. Next, for each sgRNA, we calculate the fold change between the least fluorescent to most fluorescent sample. Fold changes are corrected for increased variance at low mean values by computing a local *Z* score, which is calculated by ranking all the sgRNAs by mean value between the two conditions and calculating a *Z* score using the 2,000 sgRNA window around each sgRNA. These local Z scores are then used to calculate a *phenotype* and *p* value for each gene. *Phenotype* is calculated as the mean of the two sgRNA with the maximum absolute local *Z* score. The *p* value is calculated by taking the mean of all sgRNAs against a gene and comparing that to an empirical distribution of mean local *Z* score generated by 100,000 permutations of gene to sgRNA associations.

## DATA AND CODE AVAILABILITY

All data required to reproduce the results of the paper, including the full raw results from the CRISPR screens, are provided as supplementary materials.

## ACKNOWLEDGMENTS

This work was supported by the following grants: DP2GM137416 from NIH/NIGMS, SAP#4100083086 from PA DOH and R03NS111447-01 from NINDS awarded to O.S.. Parts of Figure 1 were created in BioRender (ODriscoll, E. (2025) https://BioRender.com/f36g430).

## AUTHOR CONTRIBUTIONS

Conception of this work is attributed to B.L.D. and O.S. Experiments were performed by E.E.O., S.A., and J.F.L. Screen data analysis was performed by E.E.O. The initial manuscript draft was written by E.E.O. and O.S., and E.E.O., S.A., B.L.D., and O.S. provided edits.

## DECLARATION OF INTERESTS

B.L.D. serves on the advisory board of Latus Biosciences, Patch Bio, Spirovant Biosciences, Resilience, and Carbon Biosciences and has sponsored research unrelated to this work from Roche, Latus, and Spirovant. Authors have filed a patent related to this manuscript through the Children's Hospital of Philadelphia.

## SUPPLEMENTAL INFORMATION

Supplemental information can be found online at https://doi.org/10.1016/j.omtm.2025.101408.

## REFERENCES

1. Au, H.K.E., Isalan, M., and Mielcarek, M. (2021). Gene Therapy Advances: A Meta-Analysis of AAV Usage in Clinical Settings. Front. Med. *8*, 809118. https://doi.org/10.3389/fmed.2021.809118.

2. Srivastava, A. (2016). In vivo tissue-tropism of adeno-associated viral vectors. Curr. Opin. Virol. *21*, 75–80. https://doi.org/10.1016/j.coviro.2016.08.003.

3. Smith, C.J., Ross, N., Kamal, A., Kim, K.Y., Kropf, E., Deschatelets, P., Francois, C., Quinn, W.J., Singh, I., Majowicz, A., et al. (2022). Pre-existing humoral immunity and complement pathway contribute to immunogenicity of adeno-associated virus (AAV) vector in human blood. Front. Immunol. *13*, 999021. https://doi.org/10.3389/fimmu.2022.999021.

4. Colella, P., Ronzitti, G., and Mingozzi, F. (2018). Emerging Issues in AAV-Mediated In Vivo Gene Therapy. Mol. Ther. Methods Clin. Dev. *8*, 87–104. https://doi.org/10.1016/j.omtm.2017.11.007.

5. Guillou, J., de Pellegars, A., Porcheret, F., Frémeaux-Bacchi, V., Allain-Launay, E., Debord, C., Denis, M., Péréon, Y., Barnérias, C., Desguerre, I., et al. (2022). Fatal thrombotic microangiopathy case following adeno-associated viral SMN gene therapy. Blood Adv. *6*, 4266–4270. https://doi.org/10.1182/bloodadvances.2021006419.

6. Lek, A., Wong, B., Keeler, A., Blackwood, M., Ma, K., Huang, S., Sylvia, K., Batista, A.R., Artinian, R., Kokoski, D., et al. (2023). Death after high-dose rAAV9 gene therapy in a patient with Duchenne's muscular dystrophy. N. Engl. J. Med. *389*, 1203–1210. https://doi.org/10.1056/NEJMoa2307798.

7. Hoggan, M.D., Blacklow, N.R., and Rowe, W.P. (1966). Studies of small DNA viruses found in various adenovirus preparations: physical, biological, and immunological characteristics. Proc. Natl. Acad. Sci. USA *55*, 1467–1474. https://doi.org/10.1073/pnas.55.6.1467.

8. Atchison, R.W., Casto, B.C., and Hammon, W.M. (1965). ADENOVIRUS-ASSOCIATED DEFECTIVE VIRUS PARTICLES. Science *149*, 754–756. https://doi.org/10.1126/science.149.3685.754.

9. Pillay, S., Meyer, N.L., Puschnik, A.S., Davulcu, O., Diep, J., Ishikawa, Y., Jae, L.T., Wosen, J.E., Nagamine, C.M., Chapman, M.S., and Carette, J.E. (2016). An essential

receptor for adeno-associated virus infection. Nature *530*, 108–112. https://doi.org/10.1038/nature16465.

10. Pillay, S., Zou, W., Cheng, F., Puschnik, A.S., Meyer, N.L., Ganaie, S.S., Deng, X., Wosen, J.E., Davulcu, O., Yan, Z., et al. (2017). Adeno-associated Virus (AAV) Serotypes Have Distinctive Interactions with Domains of the Cellular AAV Receptor. J. Virol. *91*, e00391-17. https://doi.org/10.1128/JVI.00391-17.

11. Dhungel, B.P., Bailey, C.G., and Rasko, J.E.J. (2021). Journey to the Center of the Cell: Tracing the Path of AAV Transduction. Trends Mol. Med. *27*, 172–184. https://doi.org/10.1016/j.molmed.2020.09.010.

12. Summerford, C., Johnson, J.S., and Samulski, R.J. (2016). AAVR: A Multi-Serotype Receptor for AAV. Mol. Ther. *24*, 663–666. https://doi.org/10.1038/mt.2016.49.

13. Barnes, C.R., Lee, H., Ojala, D.S., Lewis, K.K., Limsirichai, P., and Schaffer, D.V. (2021). Genome-wide activation screens to increase adeno-associated virus production. Mol. Ther. Nucleic Acids *26*, 94–103. https://doi.org/10.1016/j.omtn.2021.06.026.

14. Chung, C.-H., Murphy, C.M., Wingate, V.P., Pavlicek, J.W., Nakashima, R., Wei, W., McCarty, D., Rabinowitz, J., and Barton, E. (2023). Production of rAAV by plasmid transfection induces antiviral and inflammatory responses in suspension HEK293 cells. Mol. Ther. Methods Clin. Dev. *28*, 272–283. https://doi.org/10.1016/j.omtm.2023.01.002.

15. Anwar, M.U., Sergeeva, O.A., Abrami, L., Mesquita, F.S., Lukonin, I., Amen, T., Chuat, A., Capolupo, L., Liberali, P., D'Angelo, G., and van der Goot, F.G. (2022). ER-Golgi-localized proteins TMED2 and TMED10 control the formation of plasma membrane lipid nanodomains. Dev. Cell *57*, 2334–2346.e8. https://doi.org/10.1016/j.devcel.2022.09.004.

16. Tomita, Y., Noda, T., Fujii, K., Watanabe, T., Morikawa, Y., and Kawaoka, Y. (2011). The cellular factors Vps18 and Mon2 are required for efficient production of infectious HIV-1 particles. J. Virol. *85*, 5618–5627. https://doi.org/10.1128/JVI.00846-10.

17. Doench, J.G., Fusi, N., Sullender, M., Hegde, M., Vaimberg, E.W., Donovan, K.F., Smith, I., Tothova, Z., Wilen, C., Orchard, R., et al. (2016). Optimized sgRNA design to maximize activity and minimize off-target effects of CRISPR-Cas9. Nat. Biotechnol. *34*, 184–191. https://doi.org/10.1038/nbt.3437.

18. Shalem, O., Sanjana, N.E., Hartenian, E., Shi, X., Scott, D.A., Mikkelson, T., Heckl, D., Ebert, B.L., Root, D.E., Doench, J.G., and Zhang, F. (2014). Genome-scale CRISPR-Cas9 knockout screening in human cells. Science *343*, 84–87. https://doi.org/10.1126/science.1247005.

19. Szklarczyk, D., Kirsch, R., Koutrouli, M., Nastou, K., Mehryary, F., Hachilif, R., Gable, A.L., Fang, T., Doncheva, N.T., Pyysalo, S., et al. (2023). The STRING database in 2023: protein-protein association networks and functional enrichment analyses for any sequenced genome of interest. Nucleic Acids Res. *51*, D638–D646. https://doi.org/10.1093/nar/gkac1000.

20. Kolberg, L., Raudvere, U., Kuzmin, I., Adler, P., Vilo, J., and Peterson, H. (2023). g:Profiler-interoperable web service for functional enrichment analysis and gene identifier mapping (2023 update). Nucleic Acids Res. *51*, W207–W212. https://doi.org/10.1093/nar/gkad347.

21. Summerford, C., and Samulski, R.J. (1998). Membrane-associated heparan sulfate proteoglycan is a receptor for adeno-associated virus type 2 virions. J. Virol. *72*, 1438–1445. https://doi.org/10.1128/JVI.72.2.1438-1445.1998.

22. Kern, A., Schmidt, K., Leder, C., Müller, O.J., Wobus, C.E., Bettinger, K., Von der Lieth, C.W., King, J.A., and Kleinschmidt, J.A. (2003). Identification of a heparin-binding motif on adeno-associated virus type 2 capsids. J. Virol. *77*, 11072–11081. https://doi.org/10.1128/jvi.77.20.11072-11081.2003.

23. Pastor-Cantizano, N., Montesinos, J.C., Bernat-Silvestre, C., Marcote, M.J., and Aniento, F. (2016). p24 family proteins: key players in the regulation of trafficking along the secretory pathway. Protoplasma *253*, 967–985. https://doi.org/10.1007/s00709-015-0858-6.

24. J F Wright. Manufacturing and characterizing AAV-based vectors for use in clinical studies. Gene Ther. 15:840–848.

25. Conant, D., Hsiau, T., Rossi, N., Oki, J., Maures, T., Waite, K., Yang, J., Joshi, S., Kelso, R., Holden, K., et al. (2022). Inference of CRISPR Edits from Sanger Trace Data. CRISPR J. *5*, 123–130. https://doi.org/10.1089/crispr.2021.0113.